Combined metabolome and transcriptome analysis reveals key components of complete desiccation tolerance in an anhydrobiotic insect

Alina Ryabova[a,1] (iD), Richard Cornette[b,1] (iD), Alexander Cherkasov[a,c] (iD), Masahiko Watanabe[b,2], Takashi Okuda[d], Elena Shagimardanova[a] (iD), Takahiro Kikawada (黄川田　隆洋)[b,e,3] (iD), and Oleg Gusev[a,f,g,3] (iD)

[a]Institute of Fundamental Medicine and Biology, Kazan Federal University, 420012 Kazan, Russia; [b]Anhydrobiosis Research Group, Institute of Agrobiological Sciences, National Agriculture and Food Research Organization, Tsukuba, 305-8634 Ibaraki, Japan; [c]Center of Life Sciences, Skolkovo Institute of Science and Technology, 143028 Moscow, Russia; [d]NEMLI PROJECT LLC, Tsuchiura, 300-0023 Ibaraki, Japan; [e]Graduate School of Frontier Sciences, The University of Tokyo, Kashiwa, 277-8561 Chiba, Japan; [f]RIKEN Cluster for Science, Technology and Innovation Hub, RIKEN, 351-0198 Yokohama, Japan; and [g]RIKEN Center for Integrative Medical Sciences, RIKEN, 351-0198 Yokohama, Japan

Some organisms have evolved a survival strategy to withstand severe dehydration in an ametabolic state, called anhydrobiosis. The only known example of anhydrobiosis among insects is observed in larvae of the chironomid *Polypedilum vanderplanki*. Recent studies have led to a better understanding of the molecular mechanisms underlying anhydrobiosis and the action of specific protective proteins. However, gene regulation alone cannot explain the rapid biochemical reactions and independent metabolic changes that are expected to sustain anhydrobiosis. For this reason, we conducted a comprehensive comparative metabolome–transcriptome analysis in the larvae. We showed that anhydrobiotic larvae adopt a unique metabolic strategy to cope with complete desiccation and, in particular, to allow recovery after rehydration. We argue that trehalose, previously known for its anhydroprotective properties, plays additional vital roles, providing both the principal source of energy and also the restoration of antioxidant potential via the pentose phosphate pathway during the early stages of rehydration. Thus, larval viability might be directly dependent on the total amount of carbohydrate (glycogen and trehalose). Furthermore, in the anhydrobiotic state, energy is stored as accumulated citrate and adenosine monophosphate, allowing rapid reactivation of the citric acid cycle and mitochondrial activity immediately after rehydration, before glycolysis is fully functional. Other specific adaptations to desiccation include potential antioxidants (e.g., ophthalmic acid) and measures to avoid the accumulation of toxic waste metabolites by converting these to stable and inert counterparts (e.g., xanthurenic acid and allantoin). Finally, we confirmed that these metabolic adaptations correlate with unique organization and expression of the corresponding enzyme genes.

anhydrobiosis | metabolome | desiccation tolerance | *Polypedilum vanderplanki* | transcriptome

Water molecules form a universal substrate for all processes inside living cells and maintain the conformation of membranes and biomolecules. Severe dehydration leads to damage of cellular structures and can be lethal. If an organism cannot escape a dangerous environment it must adapt to any extreme conditions it might experience. One such adaptation is anhydrobiosis, which is the ametabolic state that occurs in some organisms in response to drought (1). Anhydrobiosis is common for the majority of plant seeds (1) and microorganisms but is also observed among a limited number of microscopic invertebrates (2). The largest anhydrobiotic animal and the only insect is "the sleeping chironomid" *Polypedilum vanderplanki* (Diptera, Chironomidae), whose larvae inhabit ephemeral rock pools in semiarid regions of western Africa. The larvae can survive almost complete water loss (up to 97% of total body mass) by entering into the anhydrobiotic state but can reestablish normal physiology within a couple of hours of rehydration. Anhydrobiosis is a natural phase in their life cycle, such that larvae can successfully withstand a series of desiccation–rehydration events. To enter into anhydrobiosis, it is necessary for larvae to follow an appropriately slow desiccation regime that normally takes about 48 h (3). Once in the anhydrobiotic state, *P. vanderplanki* larvae are able not only to survive almost complete desiccation for over 17 y but they also show outstanding cross-tolerance to various abiotic stresses, including extreme temperature fluctuation, hypoxia, high hydrostatic pressure, exposure to toxic chemicals, vacuum, and ultraviolet and different types of ionizing or electromagnetic radiation (4–7).

Over the last decade, investigations of *P. vanderplanki* larvae have resulted in an improved understanding of the machinery of anhydrobiosis, which acts at various physiological levels in the organism. In particular, unique clusters of paralogous genes including late embryogenesis abundant (LEA) proteins, thioredoxins, protein-repair methyltransferases, or hemoglobins,

Significance

Anhydrobiosis is a reversible ametabolic state that occurs in response to severe desiccation. The largest anhydrobiotic animal known is the larva of the African chironomid *Polypedilum vanderplanki*. Here, we investigated how the metabolism of larvae changes during the desiccation–rehydration cycle and how simple biochemical processes determine viability of the chironomid. Major findings suggest that, in addition to its known anhydroprotectant role, trehalose acts as a major source of energy for rehydration. Citrate and adenosine monophosphate, accumulated in the dry state, allow rapid resumption of metabolism during the recovery phase. Finally, metabolic waste is stored as stable or nontoxic compounds such as allantoin, xanthurenic acid, or ophthalmic acid that may also act as antioxidants.

which are strongly responsive to the onset of desiccation, have been identified in the *P. vanderplanki* genome (8). Comparative genome analysis showed that the congeneric species, *Polypedilum nubifer*, which is sensitive to desiccation, and other insects, such as mosquitoes of the *Anopheles* and *Aedes* genera, lack corresponding gene clusters (9). At the biochemical level, several groups of biomolecules, including LEA proteins, various antioxidants, and heat-shock proteins, act coordinately as anhydroprotectants (4, 6, 10). Trehalose is also a core determinant of desiccation tolerance in *P. vanderplanki* larvae, and its accumulation may reflect the readiness of larvae to undergo anhydrobiosis (11). In *P. vanderplanki*, as in other anhydrobiotes, this disaccharide possesses a number of anhydroprotectant features; for example, it adjusts osmotic potential in cells, protects membranes, and stabilizes macromolecules by formation of glass-like structures in the cytoplasm (12–14).

However, despite considerable knowledge of the transcriptional activity relating to anhydrobiosis, little is known about the associated nonenzymatic biochemical processes and metabolic perturbations. In the final stages of desiccation and the initial stages of rehydration there can be no enzyme activity (because water level is extremely low) and consequently homeostasis and cell structure must be maintained by small molecules. Although gene regulation is undoubtedly necessary outside this critical phase, simple biochemical and biophysical processes should predominate in a highly dehydrated "sleeping" organism.

We suggest that, either in preparation for or recovery from the dry state, the survival of the larvae is largely determined by such nonenzymatic chemical reactions. In this study, we investigated the effect of the desiccation–rehydration process on the content and proportions of metabolites in *P. vanderplanki* larvae. Our major findings suggest that 1) trehalose acts as a major source of energy sustaining the recovery of rehydrating larvae, 2) accumulated citrate and adenosine monophosphate (AMP) facilitate the rapid recovery of energy metabolism after rehydration, and 3) the accumulation of toxic waste metabolites is avoided by producing inert counterparts or potentially antioxidant compounds.

Results and Discussion

General Observations. Metabolic profiling of *P. vanderplanki* larvae revealed 266 metabolites (124 metabolites in cation mode and 142 metabolites in anion mode) across the three physiological states tested: hydrated (D0), desiccated (D48), and rehydrated (R3). A full list of the detected metabolites is available in Dataset S1 with the corresponding relative peak areas and absolute quantification for some of them. In addition to this replicated analysis on three major physiological states, single-time-course analysis was also performed throughout the desiccation and rehydration processes of *P. vanderplanki* larvae, in comparison to the lethal desiccation course in the congeneric desiccation-sensitive species *P. nubifer* (Dataset S2). According to the Human Metabolome Database 4.0 (https://hmdb.ca/) hierarchical classification (*SI Appendix*, Fig. S1), most of the metabolites identified in the main replicated analysis fell into the "organic acids and derivatives" and "nucleosides, nucleotides, and analogues" categories.

Principal component analysis (PCA) was used to determine the variability in the changes in metabolite content during the desiccation–rehydration cycle in *P. vanderplanki*. PCA showed a large spread between the three physiological states, with good agreement between the three replicates of each condition (Fig. 1*A*). In total, the first two principal components accounted for 77% of the overall variability. PC1 (43.9%) explains the general direction in concentration dynamics of the metabolites between intact hydrated larvae and larvae in the anhydrobiotic cycle (desiccation–rehydration), while PC2 (33.1%) accounts for the divergence between the dry and rehydrated stages.

The PCA loadings revealed that metabolites with high positive PC1 values demonstrate a significant increase in concentration during at least one of the stages of anhydrobiosis (Fig. 1*B*). Differences in PC2 loadings allowed the identification of three major patterns of change in metabolite content: 1) accumulation during desiccation, 2) accumulation during rehydration, and 3) accumulation during both stages of anhydrobiosis. For each of these groups, an average pattern of change was determined (Fig. 1*C*). The metabolites with the 10 highest loadings for each group are also shown; these are likely to be important for discriminating between the groups. Among these are trehalose-6-phosphate (T6P), a precursor of a compound (i.e., trehalose) with known anhydroprotective properties; intermediates of the glutathione (GSH) pathway (gamma-aminobutyric acid, gamma-glutamylcysteine, and ophthalmic acid); neuroactive intermediates of the tryptophan degradation pathway (kynurenine [KYN] and kynurenic acid [KA]); and AMP, whose accumulation is typical of *P. vanderplanki* larvae during anhydrobiosis.

Role of Trehalose in Anhydrobiosis: An Optimal Energy Resource for a Rapid Resumption of Metabolism. Metabolic profiling of *P. vanderplanki* larvae revealed significant perturbations in the levels of various carbohydrate intermediates (Fig. 2). In the metabolome of desiccated larvae, the precursor of trehalose biosynthesis, T6P, was the only sugar whose level increased (47-fold compared to hydrated larvae). As stated above, trehalose possesses a number of anhydroprotectant features (12–14) and accumulation of this disaccharide has also been determined as a core determinant of desiccation tolerance in *P. vanderplanki* larvae (11).

One way to achieve large trehalose reserves is by degradation of glycogen stored in fat body cells (15). Although glycogen is the major carbohydrate storage molecule in animals, water loss in *P. vanderplanki* shifts the carbohydrate balance toward trehalose production. Glycogen is degraded first to glucose-1-phosphate (G1P), which is then converted to glucose-6-phosphate (G6P) (15). Subsequently, trehalose is synthesized from G6P and uridine diphosphate (UDP) glucose (Fig. 2*A*). This reaction occurs in two steps, catalyzed by T6P synthase (TPS) and T6P phosphatase (TPP). In desiccated larvae, the content of G6P and UDP glucose decreased 10-fold and fivefold, respectively, while the level of UDP, an important factor in trehalose and glycogen production, increased eightfold. The activity of the respective enzymes changed as follows. The expression pattern of the TPS and TPP genes paralleled T6P accumulation and was tightly linked with water loss, with transcript levels reaching a maximum after 48-h dehydration (Fig. 2*B* and *SI Appendix*, Fig. S2). The same was observed for transcripts of the trehalose transporter (TRET1), which redistributes the disaccharide to other cells and tissues. Studies on nematode dauer larvae showed that the overexpression of TPS diverts G6P to trehalose biosynthesis, resulting in a reduction of cytosolic NADPH (16). A similar redirection of metabolic flux is likely to occur in *P. vanderplanki* larvae during desiccation (Fig. 2*A*). This is confirmed by the experimental data, showing that most glycogen present in larvae is degraded to produce trehalose during the desiccation process (Fig. 3 *A*, *Left*).

During rehydration of the larvae, the glassy trehalose matrix dissolves and free trehalose is rapidly directed back to glycogen synthesis, whose reserves are replenished after 16-h exposure to water (Fig. 3 *A*, *Right*). However, it is worth noting that the level of glycogen after rehydration is slightly lower that its level before desiccation (Fig. 3*A*). This might be due to the consumption of a substantial portion of the carbohydrate content to fuel metabolic activity. Thus, although glycogen is the main source for G6P synthesis, which in turn is converted to T6P and finally trehalose in anhydrobiotic larvae (Figs. 2 and 3), a substantial proportion of G6P is also consumed during glycolysis. This phenomenon is more clearly illustrated when larvae are subjected to consecutive
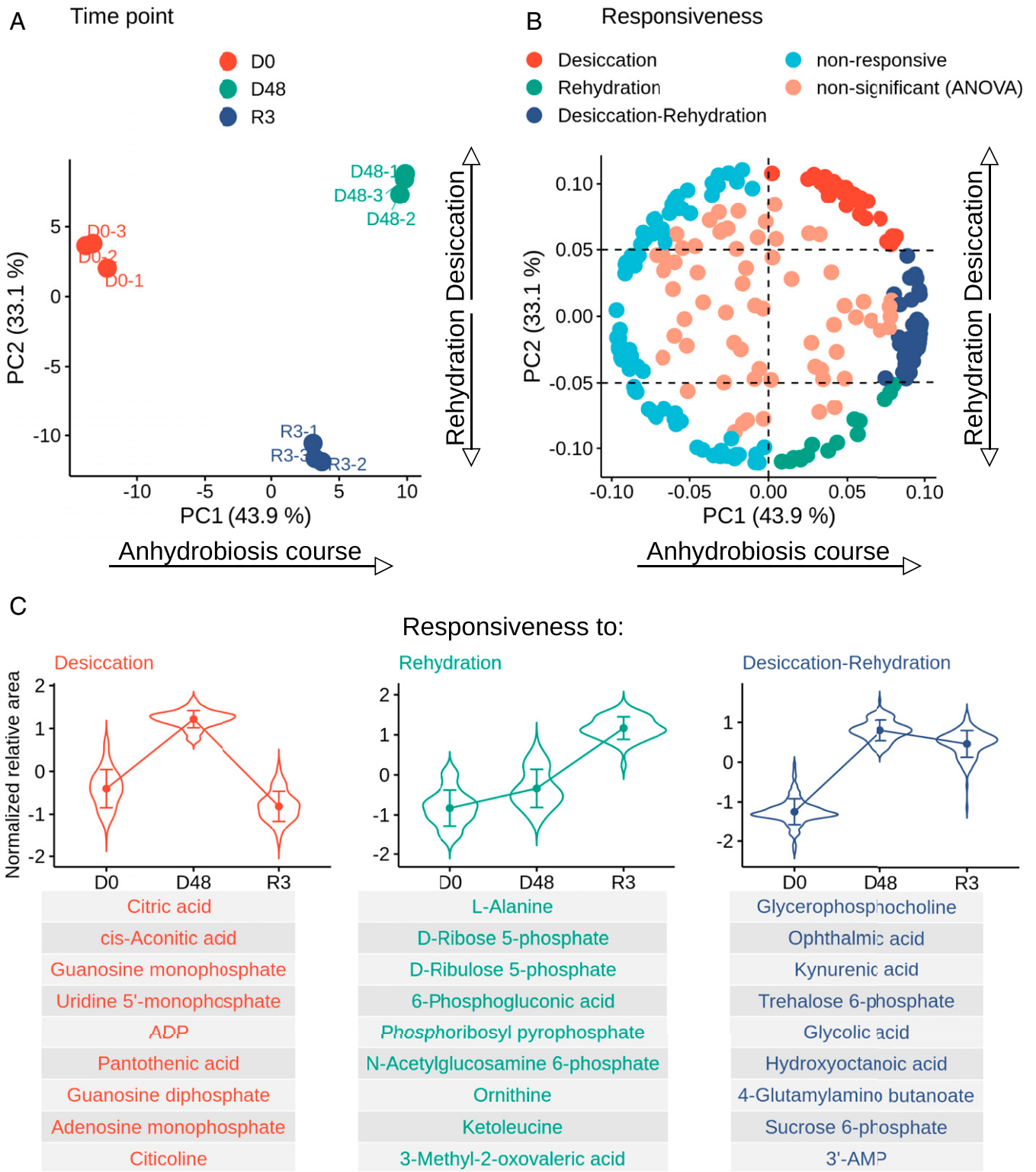
Fig. 1. Results of PCA. (*A*) PCA plot. Three replicates for each physiological state are shown as dots in different colors (see key). PC1 accounts for 43.9% of variables and explains the changes in the content of metabolites during anhydrobiosis; PC2 accounts for 33.1% of variables and shows the difference between the metabolomes of desiccated and rehydrated larvae. (*B*) Factor loading plot. Metabolites are marked with dots. The dashed lines represent threshold values (0.0 for PC1, 0.05 and −0.05 for PC2) used for classification of metabolite groups according to their responsiveness to the stage of anhydrobiosis (pattern of change in content of this metabolite). Groups of metabolites with different expression patterns are marked in different colors (see key), including ANOVA nonsignificant metabolites. (*C*) Line plots representing the average pattern of change in metabolite content for groups with different responsiveness, selected by factor loading. Error bars show SE of mean; the violins reflect the distribution of normalized abundances of metabolites. The tables below list the metabolites in each group with the 10 highest loadings.
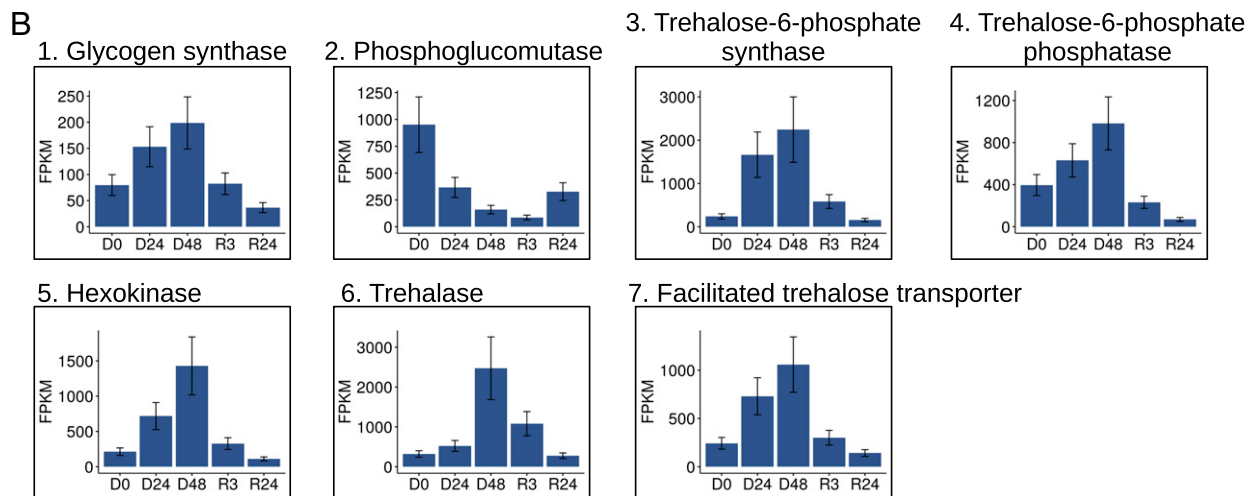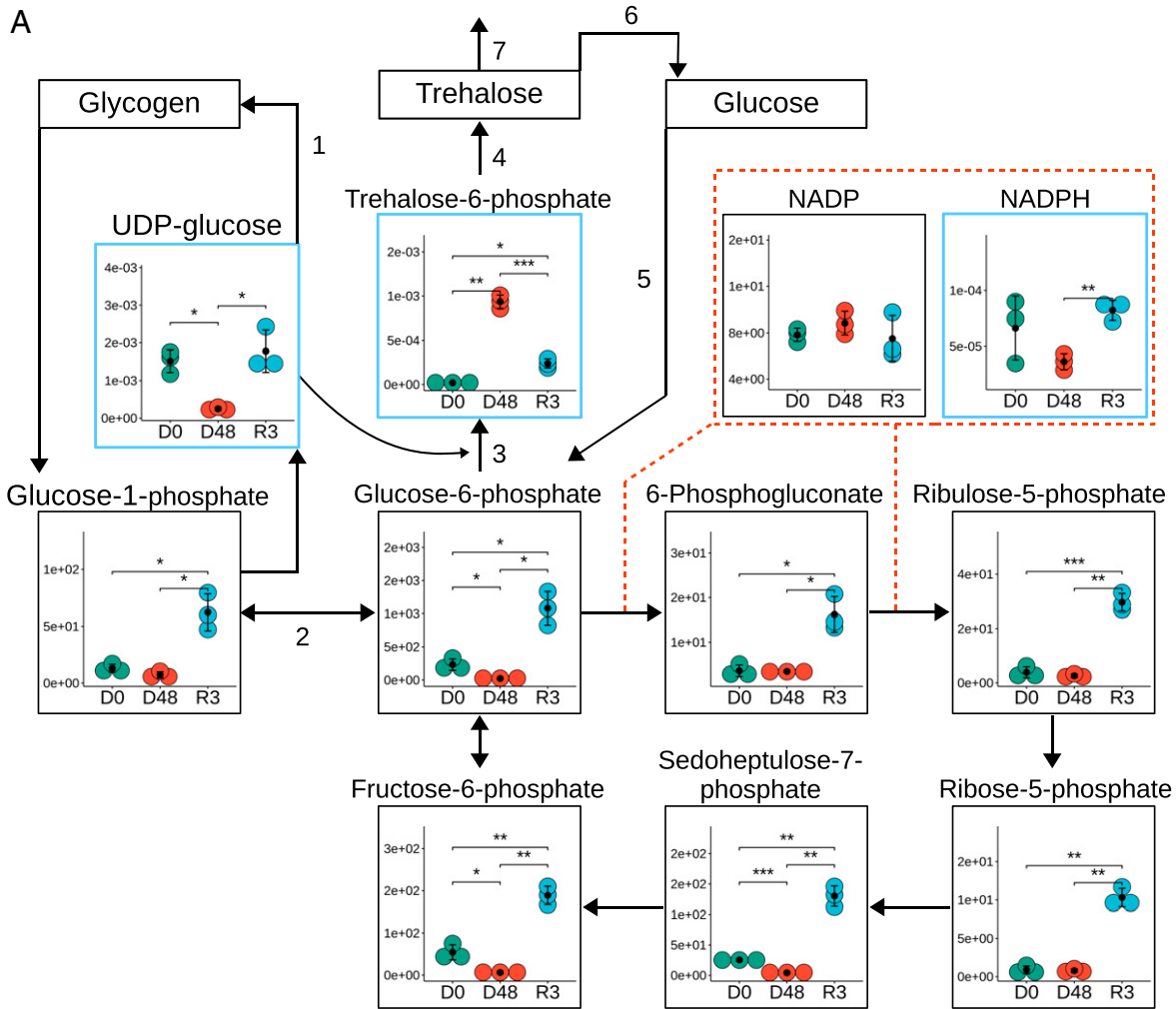
Fig. 2. (*A*) Metabolic and transcriptomic changes in carbohydrate metabolism during the desiccation–rehydration cycle of *P. vanderplanki*. The dynamics of each metabolite are shown as dot plots. Time points are indicated by colors (green, D0; red, D48; blue, R3); the averages of three replicates are marked by black dots. Error bars show SD. Asterisks indicate significance level (*<0.05, **<0.01, ***<0.001). The *y* axes show relative abundance in arbitrary units inferred from peak areas (within blue frames). For the metabolites, which had their absolute content calculated (indicated by black frames), absolute amounts in picomoles per individual are shown on the *y* axis. Enzymes and transporters involved in metabolic reactions are represented by numbers: 1) glycogen synthase; 2) phosphoglucomutase; 3) T6P synthase; 4) T6P phosphatase; 5) hexokinase; 6) trehalase; 7) facilitated trehalose transporter 1. (*B*) Expression of the enzymes and transporters cited above, obtained by transcriptome analysis at 0-h, 24-h, and 48-h desiccation (D0, D24, and D48) and 3 h and 24 h after rehydration (R3 and R24).
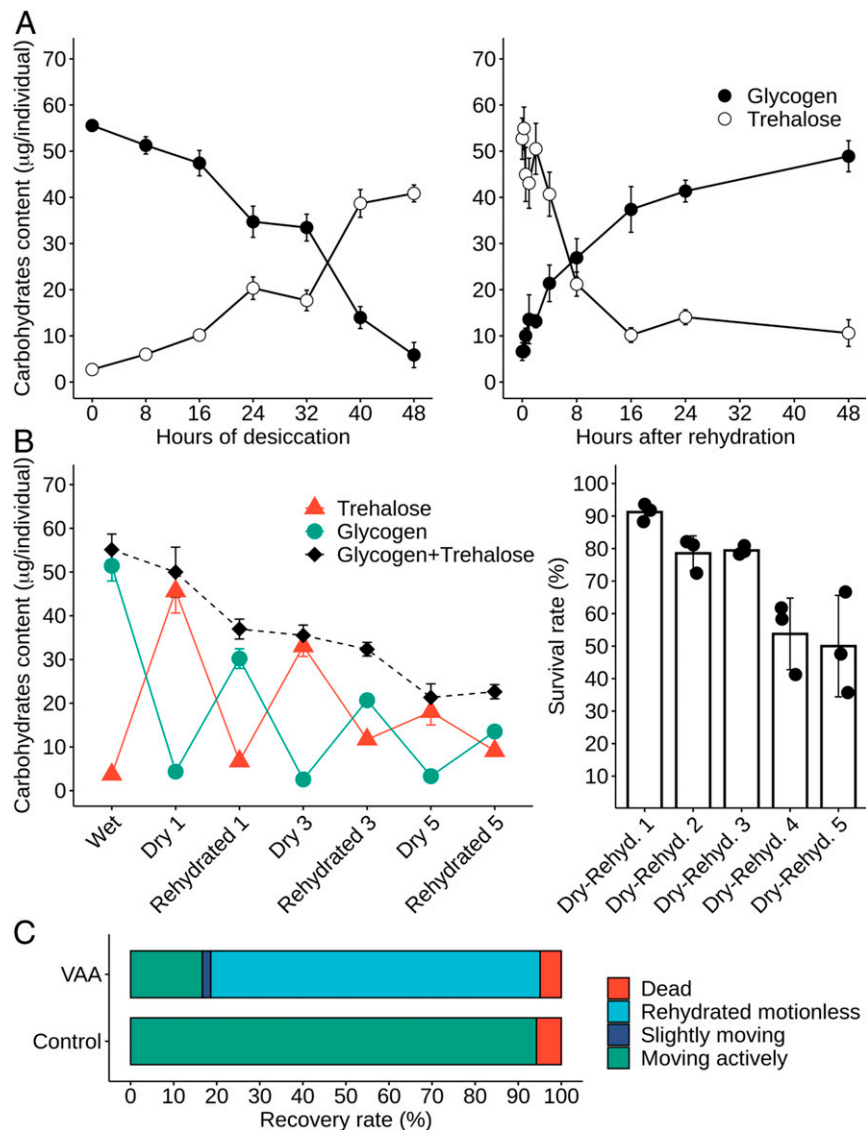
Fig. 3. (A) Monitoring of key carbohydrate levels during desiccation of *P. vanderplanki* larvae (*Left*) and during rehydration (*Right*). Trehalose content is shown as open circles and glycogen content as closed circles. Values represent the means of 8 to 15 individuals and error bars show SEM. The graph on the left was modified from ref. 15. (B) Effect of successive desiccation–rehydration cycles on carbohydrate content and on the survival of larvae. (*Left*) Monitoring of carbohydrate levels in control hydrated larvae after successive cycles of desiccation (Dry 1, 3, 5) and after the corresponding cycles of rehydration (Rehydrated 1, 3, 5). Trehalose content is shown as red triangles, glycogen content as green circles, and total carbohydrates (glycogen + trehalose) as black diamonds and a dashed line. Values represent the means of 14 to 17 individuals and error bars show SEM. (*Right*) Survival rate of larvae after one, two, three, four, and five successive cycles of desiccation and rehydration. Bars represent the means of three replicate experiments plotted with error bars showing SD. (C) Effect of trehalase inhibition on the survival of larvae 16 h after rehydration. Larvae injected either with water (control) or with trehalase inhibitor (VAA) were subjected to desiccation and subsequent rehydration. Normally rehydrated larvae moved actively, whereas unhealthy rehydrated larvae showed only slight movement or were motionless.

cycles of desiccation and rehydration, without feeding during the rehydrated phases (Fig. 3B). The total amount of carbohydrate (glycogen and trehalose) decreases little by little with each desiccation–rehydration cycle, dropping to half that of untreated larvae after five cycles (Fig. 3B). Due to this decrease in total carbohydrate content, the amount of trehalose synthesized in each desiccation cycle also decreases (Fig. 3 B, *Left*). A similar pattern of glycogen depletion during multiple bouts of dehydration was observed in the freeze-tolerant larvae of *Belgica antarctica* (17), showing that this pattern is not just a feature of anhydrobiotic midges and suggesting that tolerance to dehydration–rehydration stress is an energy-consuming challenge for chironomids, and probably insects in general. In comparison, the desiccation-sensitive chironomid *P. nubifer* is not able to mobilize its carbohydrate

reserves to produce trehalose in response to drying (*SI Appendix,* *Fig. S2*). At the same time, the survival rate of larvae after rehydration decreases along with the number of successive desiccation–rehydration cycles (Fig. 3 B, *Right*). However, although the survival of larvae after rehydration might be directly dependent on their glycogen resources, it is important to note that a substantially lower amount of trehalose than is present in larvae desiccated for the first time is sufficient to induce successful anhydrobiosis (and probably protection by vitrification), at least in a proportion of larvae (Fig. 3).

Trehalase is the enzyme that converts trehalose to glucose. Surprisingly, in the final stage of desiccation, the level of trehalase messenger RNA (mRNA) undergoes a drastic increase, perhaps so that trehalase protein production can restart

immediately after reexposure to water, thus allowing rapid glucose production. This is in addition to the trehalase protein already present in dry larvae in an inactive form, which is activated after rehydration (15). It is important to emphasize that, as larvae progress through anhydrobiosis, the transcription and translation machinery becomes fully dehydrated and therefore ceases to function. Thus, we assume that expression of the trehalase gene, which allows accumulation of corresponding mRNA in dry larvae, is a unique adaptation strategy to secure rapid postrehydration catabolism of trehalose, while the exact translational or transcriptional mechanisms by which unwanted trehalase activity is blocked in dehydrating larvae remain to be understood.

In rehydrated larvae, the content of G6P increased 48-fold compared to desiccated larvae (Fig. 2*A* and *SI Appendix*, Fig. S2). This phenomenon may be due to the action of trehalase. G6P connects several important carbohydrate pathways, including glycolysis, the pentose phosphate pathway (PPP), and the production of other sugars. PPP activation is involved in cytoprotection, where it limits oxidative damage by providing reduced NADPH. An increase in the generation of reactive oxygen species (ROS) rapidly switches the flux of G6P into the PPP (18). Similar shunting of glucose to PPP also reduces oxidative damage in nectar-feeding hawkmoths (19). As rehydration begins in *P. vanderplanki* larvae, the activity of TPS falls, allowing G6P to fuel PPP rather than glycolysis, such that NADPH returns to control levels (Fig. 2), probably enhancing the antioxidant potential of rehydrated larvae.

To illustrate the role of trehalase and check the relationship between trehalose degradation and the enhancement of antioxidative potential through PPP activation, we performed rehydration experiments with larvae treated with a trehalase inhibitor, validoxylamine A (VAA). Compared to mock-injected controls, VAA-injected larvae that were dehydrated and then assessed 16 h after rehydration showed impaired recovery, with nearly 80% of the larvae rehydrated, but motionless (Fig. 3*C*). All motionless larvae died within 48 h of rehydration. This result shows that active degradation of trehalose after rehydration is necessary for the survival of larvae. Although VAA treatment limited trehalose accumulation in dry larvae, probably due to side-effect interference with trehalose-synthesizing enzymes, it efficiently inhibited trehalose degradation after rehydration, as expected (*SI Appendix*, Fig. S3). The total antioxidant potential was investigated in control and VAA-treated larvae (*SI Appendix*, Fig. S4), but due to the side effect of VAA on trehalose accumulation in dry larvae it was not possible to clearly confirm or refute the role of trehalose degradation in oxidative stress tolerance in larvae after rehydration.

Since trehalase inhibition by VAA is expected to block mobilization of the major source of carbohydrates in rehydrated larvae (Fig. 3*A* and *SI Appendix*, Fig. S3), the death of VAA-treated larvae after rehydration can be largely explained by the impairment of glycolysis and consequently of the supply of energy (Fig. 3*C*). To verify this hypothesis, we knocked down trehalase gene expression by RNA interference (RNAi) in Pv11, a desiccation-tolerant cell line from *P. vanderplanki* (*SI Appendix*, Fig. S5). Although trehalase knockdown did not affect the viability of Pv11 cells immediately after rehydration (*SI Appendix*, Fig. S6*A*), subsequent cell growth was significantly inhibited by the treatment (*SI Appendix*, Fig. S6*B*). Since Pv11 cells are grown in a medium rich in sugars (sucrose, maltose, D-glucose, etc.), reduced flux through the glycolytic pathway cannot explain this difference in cell growth. Thus, another metabolic effect that depends on trehalose degradation must be responsible for the inhibition of cell growth in trehalase RNAi-treated Pv11 cells.

To summarize, by metabolome analysis and a series of in vivo and in vitro experiments, we have shown a not-yet-fully-investigated role of trehalose as a critical source of energy for larval survival during rehydration. Not only is trehalose accumulation necessary for formation of a protective glassy matrix in the dry state, but its rapid degradation after rehydration, which is essential for survival, promotes glycolysis and energy generation, as well as activation of the PPP, which probably attenuates damage due to oxidative stress.

Citric Acid Cycle and Energy Metabolism: Adaptive Rapid Restart upon Rehydration. The citric acid cycle (CAC) or Krebs cycle is a cyclical series of enzyme reactions in all aerobic organisms that generates energy in the form of adenosine triphosphate (ATP) (20, 21). The first product of the CAC is citric acid, which acts as a central link for many metabolic pathways and controls the energy level in cells. When in excess, citric acid inhibits glycolysis, stimulates gluconeogenesis, and impedes downstream CAC reactions (22).

During desiccation of *P. vanderplanki* larvae (Fig. 4), all CAC intermediates showed significantly reduced levels, with the exception of citrate and *cis*-aconitate, which both doubled in content. The accumulation of citric acid may have a dual impact depending on the stage of anhydrobiosis. During desiccation it could act as an emergency brake to slow down larval metabolism during the "sleeping" period. However, the accumulation of citrate could also be beneficial for survival of drought. For example, citric acid can exist in an anhydrous (water-free) form and has chelating agent properties and various antioxidant and anticoagulant effects (23–25). During rehydration, mitochondrial stocks of citrate are likely to allow a relatively rapid restart of CAC function and energy metabolism without carbohydrate input from glycolysis in the cytoplasm.

After 3-h rehydration, the levels of most CAC intermediates in *P. vanderplanki* larvae had recovered somewhat but were still lower than in control hydrated larvae (Fig. 4). However, pyruvate and lactate levels increased 7.2- and 6.9-fold, respectively, while citrate and *cis*-aconitate significantly decreased. It is worth noting that a portion of the pool of citrate can be redirected from the mitochondria to the cytoplasm to form acetyl coenzyme A, thereby fueling de novo fatty acid synthesis, lipid-based protein posttranslational modifications, or histone acetylation (26). This switch to lipid synthesis is catalyzed by ATP citrate lyase, an enzyme that is present in *P. vanderplanki* (Pv.16834) and that is up-regulated fourfold after 3-h rehydration of larvae. The relative levels of mitochondrial citrate and other CAC intermediates may indicate that during the first few hours of rehydration larvae have not yet fully reestablished normal metabolism, and that therefore energy-producing pathways are still operating at below-optimal efficiency. Alternatively, low levels of CAC intermediates may reflect a rapid turnover and increased metabolic activity. A reduction in CAC activity suggests that glycolysis plays a more prominent role during this recovery phase; similar findings have been reported for the freeze-tolerant midge *B. antarctica* during exposure to low temperature (27) and for diapause embryos of *Artemia franciscana* (28). However, our data revealed that, during the early stages of rehydration of *P. vanderplanki* larvae, glycolysis is also not fully operational and mainly fuels the PPP (Fig. 2). Regeneration of CAC intermediate levels only returned to near-normal after 12 h rehydration, when PPP activity ended, with most carbohydrate flux passing directly through glycolysis to the CAC (*SI Appendix*, Fig. S7).

Dynamics of Adenylates: Optimal Energy Storage for Rapid Reactivation. The levels of macroergic nucleoside triphosphates (ATP, cytidine 5′-triphosphate, and guanosine triphosphate) were reduced during desiccation, while almost all mono- and diphosphates levels were elevated. During rehydration, the trend in levels of nucleotides reversed. One of the clearest features of anhydrobiosis in *P. vanderplanki* larvae is the accumulation of
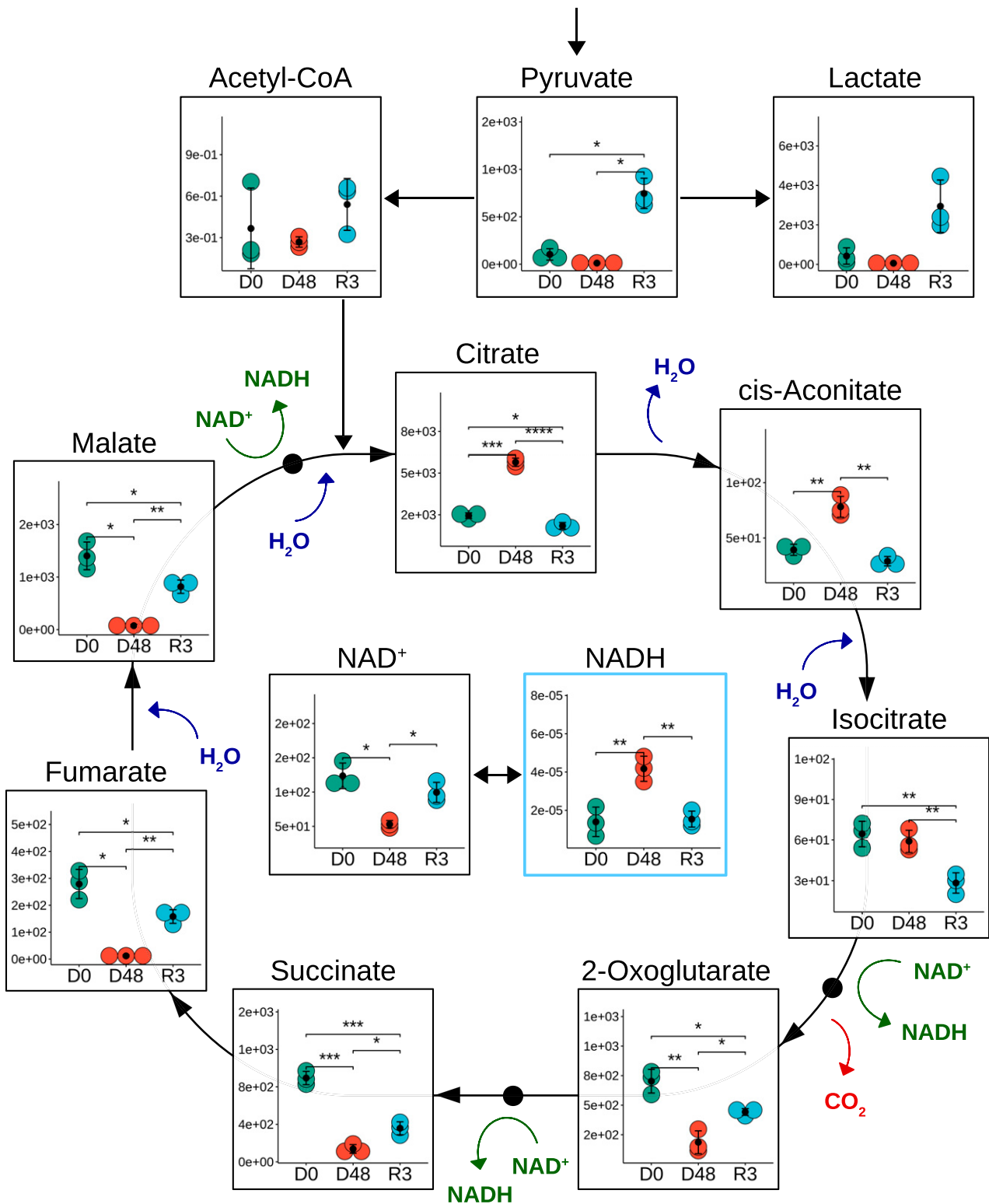
Fig. 4. Content changes in CAC intermediate metabolite levels during anhydrobiosis of *P. vanderplanki* larvae. Data are shown as described for Fig. 2. Asterisks indicate significance level (*<0.05, **<0.01, ***<0.001, ****<0.0001).

AMP and adenosine 5′-diphosphate (ADP) during desiccation (Fig. 5*A*).

In hibernating and estivating animals, metabolic depression reduces mitochondrial respiration, leading to a decrease in ATP production and an accumulation of AMP (29). The absence of additional phosphate groups in AMP probably makes it more stable and hence preferable as an energy-storage molecule in the dehydrated organism. In other anhydrobiotes, especially in dry plant seeds, metabolic depression due to desiccation also leads to the shut-down of ATP production and as a result most adenylate
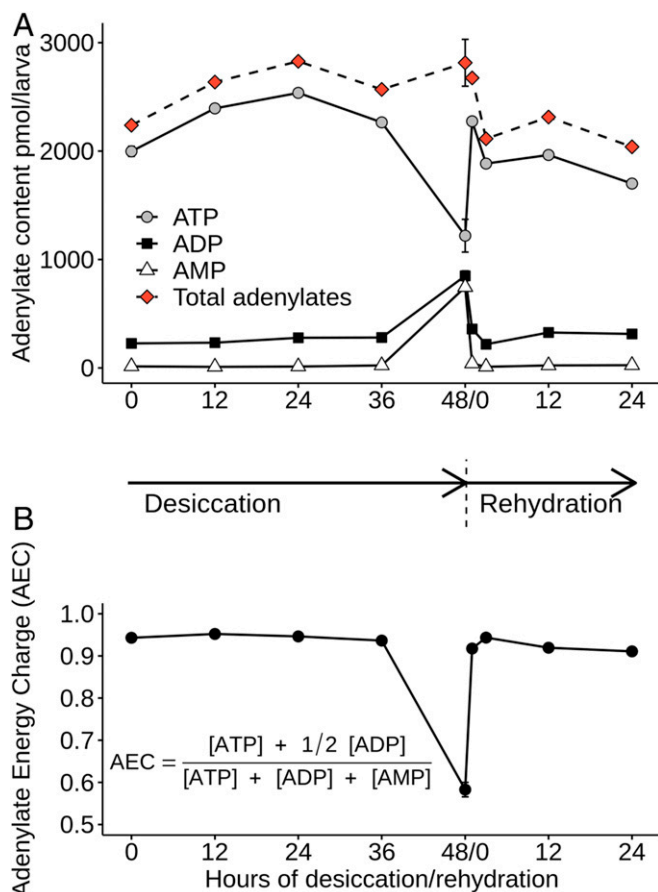
Fig. 5. (A) Fluctuations in the content of each adenylate. (B) The AEC ratio during desiccation and subsequent rehydration. SD is shown for D0 and D48/R0 samples, which were obtained in duplicate.

is stored as AMP in the dry state (30). Early in the seed rehydration process, where AMP concentration is high, the enzyme adenylate kinase catalyzes the production of ADP from AMP and ATP. In turn, this ADP fuels ATP production through mitochondrial respiration, leading to the resumption of metabolism (30). In *P. vanderplanki*, a similar mechanism is likely to occur, but in contrast to dry plant seeds, in which most ATP is converted to AMP, anhydrobiotic larvae still retain half of their ATP compared to the hydrated state. Diapause embryos from *A. franciscana* behave similarly, retaining 20% of the ATP present in postdiapause embryos (28). In fact, dry *P. vanderplanki* larvae need sufficient ATP during storage to sustain early metabolic activity and muscular activity, which can sometimes be observed as soon as a few minutes after rehydration. The adenylate energy charge (AEC) ratio in the dry state drops to only 0.6 (Fig. 5B), which is a value generally observed under stress conditions such as fermentation (30) but which corresponds here to ametabolic anhydrobiosis. It is worth noting that normal respiration and mitochondrial activity, as indicated by a high AEC ratio, are observed until the very last hours of desiccation and recover quickly within the first hour of rehydration (Fig. 5B). During rehydration, a high AMP:ATP ratio in cells activates AMP-activated protein kinase, the principal regulator of energy homeostasis, thereby promoting catabolic processes that generate ATP (31).

Accumulation of Nontoxic Metabolites and Antioxidants. Whereas the fluctuations of amino acid levels (*SI Appendix,* Fig. S8) were difficult to interpret, except for some amino acids with protective

properties such as proline (32, 33), the changes in levels of related amino acid degradation products hinted at putative mechanisms for the safe control of metabolic waste.

For example, the degradation of nitrogenous amino acids fuels the urea cycle, and in the metabolome of *P. vanderplanki* related compounds, such as uric acid, allantoin, and allantoic acid, were all among the intermediates whose abundance was most increased during anhydrobiosis (Dataset S1 and Fig. 6A), with allantoin the most highly represented. The conversion of uric acid to allantoin is catalyzed by the enzyme uricase. In the transcriptome of *P. vanderplanki,* the uricase-coding gene was markedly up-regulated after 24-h desiccation (Fig. 6A).

Many studies suggest multiple roles of allantoin beyond nitrogen recycling. For example, it is implicated in prolonging lifespan in *Caenorhabditis elegans* (34) and enhancing resistance to abiotic stresses in *Arabidopsis thaliana* (35). It is highly likely that excreted nitrogen can be stored in the form of nontoxic allantoin, which potentially could have antioxidant properties. Notably, the metabolites downstream of allantoin, allantoic acid and especially toxic urea, showed highly elevated levels only 12 h after rehydration (*SI Appendix,* Fig. S9), when the excretion system of the larvae is expected to resume normal activity. In comparison, larvae of *P. nubifer* accumulate urea early in response to desiccation (*SI Appendix,* Fig. S9) and this could be one of the factors leading to their subsequent death. The production of allantoin could therefore be an evolutionary advantage during anhydrobiosis, when excretion is not possible, and thus it may represent one of the adaptations to severe dehydration.

GSH, which is the most abundant and ubiquitous low-molecular-weight thiol in cells, plays a crucial role in antioxidant defense and the detoxification of xenobiotics (36). Earlier studies showed that even before the induction of anhydrobiosis, *P. vanderplanki* larvae maintain a high level of various anhydroprotectants and antioxidants, including GSH (9). When metabolism slows down and rapid enzyme/protein biosynthesis becomes difficult, the GSH system should allow fast neutralization of ROS without enzyme reactions. However, changes in GSH and cysteine levels were not meaningful, although the content of the main intermediate of GSH synthesis, γ-glutamylcysteine (γ-Glu-Cys), was noticeably higher during rehydration of desiccated larvae than in control, hydrated larvae (Fig. 6B). Production of γ-Glu-Cys is catalyzed by glutamate-cysteine ligase (GCL), which governs the rate-limiting step of GSH synthesis and which depends on the availability of cysteine (37). Analysis of the anhydrobiosis-related transcriptome revealed that GCL was up-regulated, with levels peaking soon after rehydration. However, the second enzyme in the GSH synthesis pathway, glutathione synthetase, did not show any significant changes in expression (Fig. 6B). It has been reported that γ-Glu-Cys can efficiently scavenge ROS independently of cellular GSH status, acting as a peroxidase cofactor (38). At the same time, activation of GSH biosynthesis simultaneously initiates the production of ophthalmic acid (OA), which can be a sensitive indicator of GSH depletion and is used as biomarker of oxidative stress (39). OA levels increased 13-fold in the metabolome of desiccated *P. vanderplanki* larvae and stayed high during the first few hours of rehydration (Fig. 6B and *SI Appendix,* Fig. S10). OA is a tripeptide GSH analog with L-2-aminobutyrate (2-AB) in place of the cysteine group. The physiological role of ophthalmate is not entirely clear, but it is assumed that OA possesses antioxidant properties and exerts a protective function due to its similarity to GSH (40). OA can be synthesized from γ-glutamyl-2-aminobutyric acid (γ-Glu-2AB), using the same enzymes as GSH biosynthesis. Notably, γ-Glu-2AB was detected only in the metabolome of fully desiccated larvae and in the early stages of rehydration (*SI Appendix,* Fig. S10). Increasing OA biosynthesis during the desiccation–rehydration cycle might therefore help to reduce the pressure on intracellular GSH levels during oxidative stress.
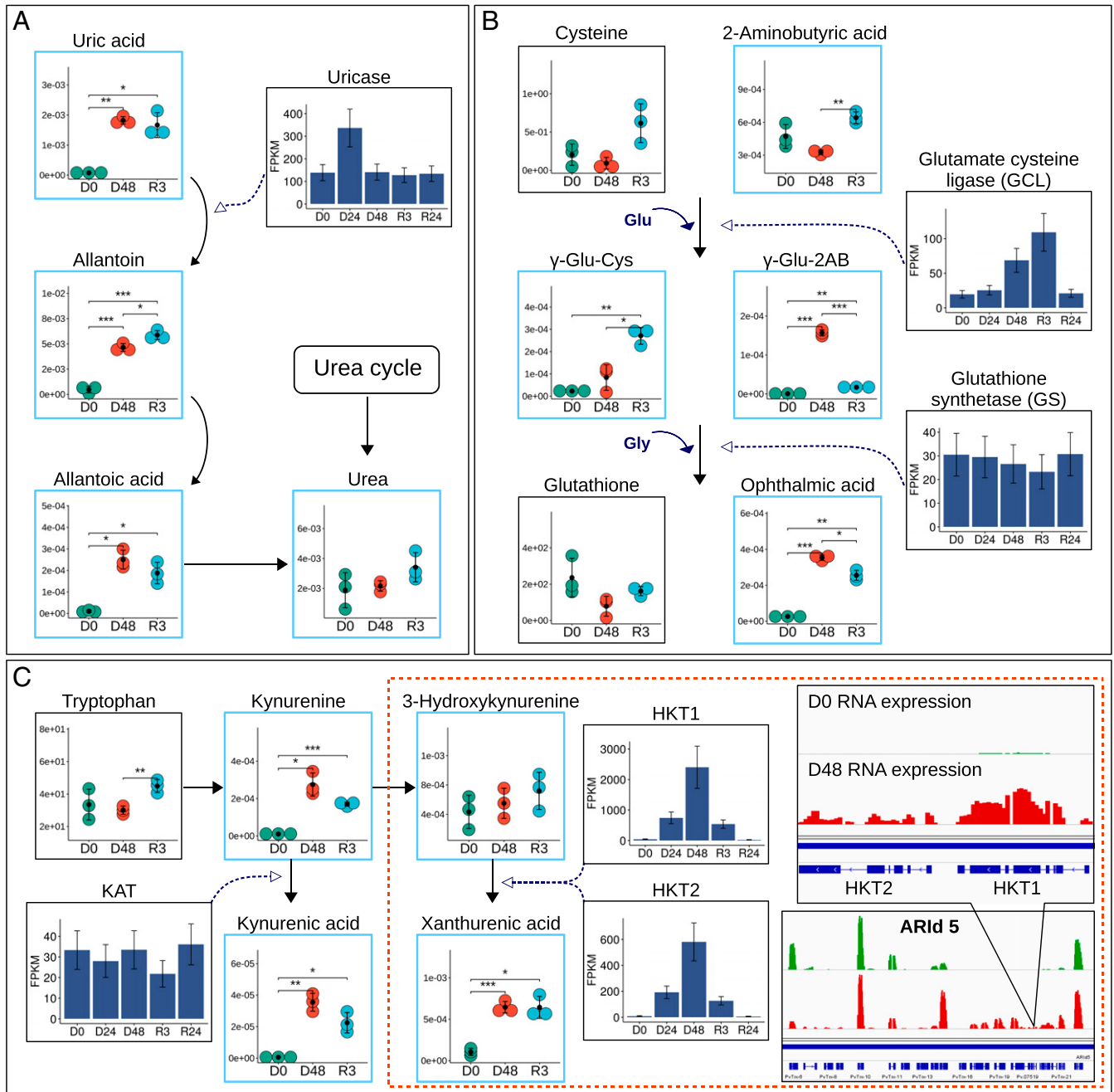
Fig. 6. (*A*) Uricase expression pattern and related metabolic profiling of uric acid degradation pathway. (*B*) GSH synthesis and the alternative OA pathway: levels of GSH, pathway intermediates, and related enzymes. (*C*) KYN pathway and expression patterns of related enzymes. Boxes on the right show the localization of putative HKT genes in anhydrobiosis-related gene island 5 (ARId 5), where the green and red data points indicate RNA-seq coverage at the D0 and D48 time points, respectively. Metabolome data are shown as described for Fig. 2. Asterisks indicate significance level (*<0.05, **<0.01, ***<0.001). Enzyme expression patterns were obtained by transcriptome analysis at 0 h, 24 h, 48 h desiccation (D0, D24, and D48) and 3 h and 24 h after rehydration (R3 and R24).

Among the most anhydrobiosis-responsive metabolites were intermediates of the tryptophan oxidation pathway: KYN and KA. The level of KYN increased markedly by about 26-fold during desiccation (Fig. 6*C*). KA was detected only in dried and rehydrated larvae. The breakdown of tryptophan via kynurenines is accompanied by the production of several neuroactive intermediates. Some of them, including KA at its normal physiological level, possess neuroprotectant activity, while other derivatives of KYN, such as 3-hydroxykynurenine (3-HK), are easily oxidized and provoke the generation of reactive radicals (41, 42).

Accordingly, it has been shown that an excessive accumulation of kynurenines, especially 3-HK, exerts a severe neurotoxic effect and induces motor dysfunction in adult insects (43). Unlike vertebrates, insects do not have kynureninase, so they are unable to hydrolyze both KYN and highly toxic 3-HK to anthranilic acid and 3-hydroxyanthranilic acid. However, chemically reactive 3-HK can be converted to the chemically stable and nontoxic compound xanthurenic acid (XA) (41). During the desiccation–rehydration cycle in *P. vanderplanki*, the 3-HK content did not vary significantly, while XA levels increased 6.1 times during desiccation, with

a moderate decrease in the first hours of rehydration (Fig. 6*C* and *SI Appendix*, Fig. S11). The constancy of the 3-HK level, along with the accumulation of its product, XA, under extremely harsh conditions such as occur during anhydrobiosis suggests that kynurenine aminotransferase (KAT), which catalyzes the processing of KYN to KA and 3-HK to XA in mammals (44, 45), remains highly effective during drought, which may be important for survival. In insects there is insufficient information about the enzymes involved in the transamination reaction of KYN and 3-HK, but it is usually assumed that a similar form of KAT is present (41). In *P. vanderplanki*, the expression level of KAT was low and did not change significantly during anhydrobiosis, which may indicate another pathway for 3-HK utilization. An alternative route for XA biosynthesis was suggested by Han et al. (46) in the yellow fever mosquito, *Aedes aegypti*. They found that alanine glyoxylate transaminase in the mosquito efficiently converted 3-HK to XA and thus renamed this enzyme 3-hydroxykynurenine transaminase (HKT). A search for orthologous genes in the *P. vanderplanki* genome revealed two genes, annotated as serine-pyruvate aminotransferase, but which are very similar to *Ae. aegypti* HKT and probably convert 3-HK to XA. These genes are located in tandem as a result of a duplication event. In addition, both copies form part of one of the unique genome islands found in *P. vanderplanki* (anhydrobiosis-related islands, ARIds), which exhibit a strong transcriptional response to desiccation (Fig. 6*C*). As previous studies revealed (9), the basic mechanism of ARId formation is massive duplication and reshuffling of the most beneficial genes, all showing a similarly enhanced expression pattern in response to desiccation. Hence, the duplication, specific localization, and regulation of the putative HKT genes in *P. vanderplanki* highlight the importance of 3-HK utilization for the production of inert XA during anhydrobiosis.

Conclusions

Metabolic profiling showed significant perturbations in the metabolism of anhydrobiotic *P. vanderplanki* larvae during the desiccation–rehydration cycle, providing insight into potentially important and adaptive functions relating to anhydrobiosis. As expected, T6P, as a precursor of trehalose, was the compound whose content increased the most in desiccated larvae, because high levels of trehalose are crucial for the viability of *P. vanderplanki* during anhydrobiosis. Besides de novo synthesis, a considerable portion of the accumulated trehalose derives from stored glycogen. We consider that in addition to the widely recognized role of trehalose as an anhydroprotectant, it also serves as an energy carrier, which is dispersed throughout the body of dehydrating larvae and is thus readily available on rehydration. This function, that is, trehalose degradation, is essential for the survival of rehydrating larvae: During the first few hours after rehydration, trehalose is rapidly converted to glucose, after which it mainly fuels the PPP, presumably to restore redox homeostasis (Fig. 7).

During the early stages of rehydration, glycolysis and the CAC are probably not fully operational, while during desiccation the CAC is impeded at the stage of citric acid isomerization, resulting in the accumulation of citrate. In the anhydrobiotic midge, a stock of citric acid may be an additional advantage due to its ability to be stored in a water-free form and because of its preservative properties. Similarly, a high AMP:ATP ratio is a particular feature of desiccated larvae. Thus, our results suggest that during rehydration the accumulated AMP, residual ATP, and citrate act in concert, allowing energy metabolism to resume faster and independently of glycolysis. As expected from our starting hypothesis, such rapid biochemical reactions are essential for successful anhydrobiosis, especially during the rehydration process, when transcriptional and translational activities that sustain de novo metabolic reactions are still insufficient to cope with the extraordinarily stressful transition that is rehydration.

In addition to the action of major known anhydroprotectants, important changes occur on a biochemical level which reduce the buildup of toxic compounds. Stocks of excess nitrogenous compounds prior to excretion accumulate mostly in the form of allantoin, which may also have benefits as an antioxidant. The KYN pathway predominantly switches to the generation of nontoxic XA. Accumulation of OA seems to be connected with reinforcement or conservation of the GSH system.

In summary, the major findings on the metabolic changes in *P. vanderplanki* larvae during anhydrobiosis and after rehydration can be distilled into three main points: 1) Trehalose acts as a source of energy and, putatively, redox power to support the recovery of rehydrating larvae; 2) accumulated citrate and AMP should facilitate the recovery of energy metabolism during early rehydration; and 3) accumulated OA, XA, allantoin, and polyamines may serve as antioxidants or nontoxic alternatives for waste compounds. These hypotheses suggest new avenues for further research into the mechanisms of anhydrobiosis and potentially for desiccation engineering and dry-storage applications.

Materials and Methods

Insect Rearing and Sample Preparation for Metabolic Profiling. *P. vanderplanki* larvae were reared on a 1% agar diet, containing 2% commercial milk, under controlled conditions (13 h light:11 h dark; temperature 27 to 28 °C) according to the established protocol (3). The induction of anhydrobiosis by desiccation was described previously (11); for a detailed description, see *SI Appendix*. Larvae for metabolome analysis were sampled according to the time (hours) spent in the desiccator (D48: 48-h desiccation, i.e., anhydrobiotic dry larvae) or spent after rehydration (R3: 3-h rehydration); untreated wet larvae were used as a control (D0). For each treatment 50 larvae were used. Metabolome analysis was performed with three biological replicates.

Measurement of Metabolites. Measurement of metabolites was carried out by Human Metabolome Technologies, Inc. (HMT; Tsuruoka, Yamagata, Japan). Larval samples (50 individuals each) were homogenized in 500 μL methanol containing internal standards and then, after mixing with 500 μL chloroform and 200 μL water, samples were centrifuged at 2,300 × *g* for 5 min. The aqueous supernatant fraction was filtered with 5-kDa exclusion filter tubes (UltraFree-MC PLHCC HMT; Millipore) and then dried. Samples were recovered into 50 μL MilliQ water, prior to metabolite analysis using capillary electrophoresis time of flight-mass spectrometry (CE-TOFMS; Agilent Technologies) in two modes for cationic and anionic metabolites. All metabolites were analyzed using a fused silica capillary (50 μm internal diameter; 80 cm total length). For the anionic analysis, the sample was injected at a pressure of 50 mbar for 25 s; the applied voltage was set at 30 kV. Cationic metabolite samples were injected at a pressure of 50 mbar for 10 s; the applied voltage was set at 27 kV. Both spectrometers were scanned from mass-to-charge (*m/z*) 50 to 1,000. Peaks detected in the CE-TOFMS analysis were extracted using automatic integration software MasterHands ver. 2.9.0.9 (Keio University, Japan). The peaks were annotated with the 272 specified putative metabolites from the package in the HMT metabolite database on the basis of their migration time (MT) in CE and *m/z* values determined by TOFMS. The tolerance range for the peak annotation was configured at 0.5 min for MT and 50 parts per million for *m/z*. The identification and quantification of each metabolite was performed according to a previously reported method (47).

Metabolome Data Analysis. Analysis of metabolic profiling data was performed using the MetaboAnalyst 4.0 R package (https://www.metaboanalyst. ca/). The dataset of detected compounds was filtered to remove metabolites with 2/3 missing values. To replace missing concentration values of low-abundance metabolites (below detection threshold), marked as "ND," we used half the minimum positive values in the original data. To identify general trends in content changes and to detect metabolites with similar pattern of change we used PCA. For PCA the normalization procedure was applied using generalized log transformation and normalization by a pooled sample from control (D0) group. Statistical analysis was conducted with one-way ANOVA to identify metabolites, which significantly changed at least at one time point. For pairwise comparison between time points, the Fischer test was applied. For reconstruction of metabolic pathways and integration
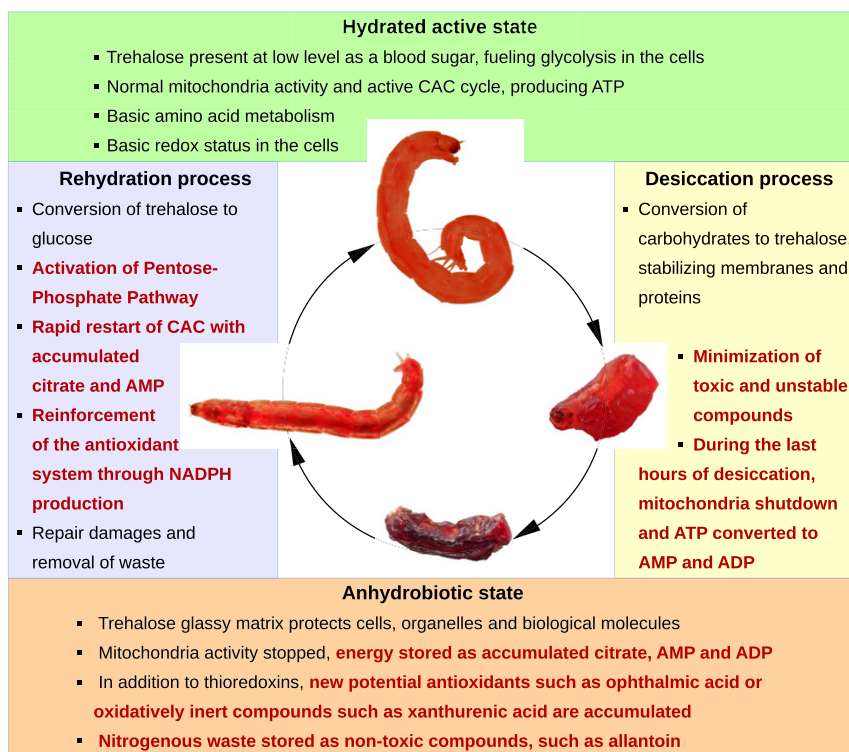
Fig. 7. Summary of the major metabolic events observed during desiccation and rehydration of *P. vanderplanki* larvae that allow successful anhydrobiosis. Features described in this study are highlighted in bold red.

with transcriptomics data, we used KEGG (Kyoto Encyclopedia of Genes and Genomes) PATHWAY Database on available species of Diptera together with a BLASTp search.

Transcriptome Analysis. Larval samples were prepared at five time points (three replicates each) to characterize the desiccation–rehydration cycle in *P. vanderplanki*. Total RNA was extracted with TRIzol (Life Technologies) and purified with a RNeasy mini kit (QIAGEN). RNA quality was assessed with a Bioanalyzer (Agilent Technologies), and RNA was quantified with a Qubit 2.0 fluorometer (Thermo Fisher). A first-strand complementary DNA library was synthesized with a TruSeq RNA sample prep kit v2 (Illumina) and sequenced on an Illumina HiSEq. 1500 with a length of 51 nucleotides using a single-end sequencing protocol in the rapid mode at the Functional Genomics Facility of the National Institute for Basic Biology (Okazaki, Japan). Read quality was checked with FastQC and the reads were preprocessed by cutting the adaptor region and the first 20 bases from the 3′-end if these bases represented a poly(A) tail. RNA-sequencing (RNA-seq) reads were mapped to the reference *P. vanderplanki* genome using TopHat 2 with default settings. Cufflinks was used to assemble RNA-seq reads into transcripts, using existing gene model information, and to estimate transcript abundances. Cuffdiff was used to find significant changes in transcript expression between time points.

Trehalose Quantification. Following the procedure described in Watanabe et al. (3), larvae were individually homogenized in 200 µL 80% ethanol containing 0.1 mg sorbitol as an internal control. After membrane filtration of the soluble fraction (pore size 0.45 µm), the supernatant was dried overnight in a centrifugal concentrator (VC-360; TAITEC) linked to a cold trap (VA-300; TAITEC) and a pump (GLD-135; ULVAC KIKO). Dried residues were dissolved in 500 µL MilliQ water (Merck Millipore) and then samples were analyzed on a Shimadzu HPLC system (LC-10A system,; Shimadzu) equipped with a guard column (Shim-pack SRC-C, 4.0 mm × 50 mm; Shimadzu) connected to an analytical column (Shim-pack SCR-101C, 7.9 mm × 300 mm; Shimadzu) and a reflective index detector (RID-6A; Shimadzu). The columns were heated to 80 °C and the flow rate of the mobile phase (MilliQ) was 0.8 mL/min. The injection volume was set at 10 or 20 µL. Standard trehalose and sorbitol solutions were prepared in MilliQ water in the range 1 to

5,000 µg/mL. From the HPLC profile trehalose could be quantified, at least in the higher range.

Glycogen Quantification. The determination of glycogen content in *P. vanderplanki* larvae was performed as described previously (15). Briefly, after larvae were individually homogenized in 200 µL 80% ethanol as described above, the insoluble fractions were boiled for 30 min in the presence of 30% KOH. Glycogen was then precipitated in 80% ethanol, followed by centrifugation at 20,000 × g for 15 min at room temperature. The resulting glycogen pellets were dissolved in distilled water prior to glycogen content determination following the phenol–sulfuric acid method (48).

Trehalase Inhibitor Treatment. Fourth instar *P. vanderplanki* larvae were injected with about 100 nL of a 100 µg/µL solution of the trehalose inhibitor VAA (BioApply Co., Ltd.) or alternatively with 100 nL water (solvent for VAA) as a control. Injections were performed under a stereomicroscope (Leica MZ16A) with a micromanipulator (M300; Suruga Seiki) piloted by computer (Endeavor; Epson; Windows XP operating system) and with an electronic air injector (IM-30; Narishige) connected to a silent air compressor (SC-71; Hitachi). The glass capillaries (GNP_IB 1.0 × 0.6 mm, ST Science) used for microinjection were pulled with a PC-10 puller (Narishige) and the tip of the capillaries was physically broken so as to smoothly deliver the vector solution without lethally wounding the larvae. Control and VAA-treated larvae were allowed to recover for 24 h and the survivors were desiccated according to the procedure described above. After 5-d desiccation, anhydrobiotic larvae were rehydrated with distilled water and the behavior of rehydrating larvae was monitored for 16 h before larvae were killed for subsequent experiments.

Data Availability. All raw metabolome data are available as Datasets S1 and S2.

1. O. Leprince, J. Buitink, Introduction to desiccation biology: From old borders to new frontiers. *Planta* **242**, 369–378 (2015).
2. M. Watanabe, Anhydrobiosis in invertebrates. *Appl. Entomol. Zool.* **41**, 15–31 (2006).
3. M. Watanabe, T. Kikawada, N. Minagawa, F. Yukuhiro, T. Okuda, Mechanism allowing an insect to survive complete dehydration and extreme temperatures. *J. Exp. Biol.* **205**, 2799–2802 (2002).
4. R. Cornette, T. Kikawada, The induction of anhydrobiosis in the sleeping chironomid: Current status of our knowledge. *IUBMB Life* **63**, 419–429 (2011).
5. M. Watanabe *et al.*, Estimation of radiation tolerance to high LET heavy ions in an anhydrobiotic insect, *Polypedilum vanderplanki*. *Int. J. Radiat. Biol.* **82**, 835–842 (2006).
6. O. Gusev *et al.*, Anhydrobiosis-associated nuclear DNA damage and repair in the sleeping chironomid: Linkage with radioresistance. *PLoS One* **5**, e14008 (2010).
7. A. Ryabova *et al.*, Genetic background of enhanced radioresistance in an anhydrobiotic insect: Transcriptional response to ionizing radiations and desiccation. *Extremophiles* **21**, 109–120 (2017).
8. R. Cornette *et al.*, Identification of anhydrobiosis-related genes from an expressed sequence tag database in the cryptobiotic midge *Polypedilum vanderplanki* (Diptera; Chironomidae). *J. Biol. Chem.* **285**, 35889–35899 (2010).
9. O. Gusev *et al.*, Comparative genome sequencing reveals genomic signature of extreme desiccation tolerance in the anhydrobiotic midge. *Nat. Commun.* **5**, 4784 (2014).
10. P. V. Mazin *et al.*, Cooption of heat shock regulatory system for anhydrobiosis in the sleeping chironomid *Polypedilum vanderplanki*. *Proc. Natl. Acad. Sci. U.S.A.* **115**, E2477–E2486 (2018).
11. M. Watanabe, T. Kikawada, T. Okuda, Increase of internal ion concentration triggers trehalose synthesis associated with cryptobiosis in larvae of *Polypedilum vanderplanki*. *J. Exp. Biol.* **206**, 2281–2286 (2003).
12. J. H. Crowe, L. M. Crowe, D. Chapman, Preservation of membranes in anhydrobiotic organisms: The role of trehalose. *Science* **223**, 701–703 (1984).
13. L. Rebecchi, T. Altiero, R. Guidetti, Anhydrobiosis: The extreme limit of desiccation tolerance. *Invertebrate Surviv. J.* **4**, 65–81 (2007).
14. M. Sakurai *et al.*, Vitrification is essential for anhydrobiosis in an African chironomid, *Polypedilum vanderplanki*. *Proc. Natl. Acad. Sci. U.S.A.* **105**, 5093–5098 (2008).
15. K. Mitsumasu *et al.*, Enzymatic control of anhydrobiosis-related accumulation of trehalose in the sleeping chironomid, *Polypedilum vanderplanki*. *FEBS J.* **277**, 4215–4228 (2010).
16. S. Penkov *et al.*, Integration of carbohydrate metabolism and redox state controls dauer larva formation in *Caenorhabditis elegans*. *Nat. Commun.* **6**, 8060 (2015).
17. N. M. Teets, Y. Kawarasaki, R. E. Lee Jr., D. L. Denlinger, Energetic consequences of repeated and prolonged dehydration in the Antarctic midge, *Belgica antarctica*. *J. Insect Physiol.* **58**, 498–505 (2012).
18. M. L. Cheng *et al.*, Sedoheptulose-1,7-bisphospate accumulation and metabolic anomalies in hepatoma cells exposed to oxidative stress. *Oxid. Med. Cell. Longev.* **2019**, 5913635 (2019).
19. E. Levin, G. Lopez-Martinez, B. Fane, G. Davidowitz, Hawkmoths use nectar sugar to reduce oxidative damage from flight. *Science* **355**, 733–735 (2017).
20. J. W. Locasale, L. C. Cantley, Metabolic flux and the regulation of mammalian cell growth. *Cell Metab.* **14**, 443–451 (2011).
21. K. Sawa *et al.*, Krebs cycle intermediates protective against oxidative stress by modulating the level of reactive oxygen species in neuronal HT22 cells. *Antioxidants* **6**, E21 (2017).
22. P. Icard, L. Poulain, H. Lincet, Understanding the central role of citrate in the metabolism of cancer cells. *Biochim. Biophys. Acta* **1825**, 111–116 (2012).
23. P. N. Campbell, *Biochemistry Illustrated*, (Churchill Livingstone, ed. 4, 2000).
24. H. Poerwono *et al.*, "Citric acid" in *Analytical Profiles of Drug Substances and Excipients*, K. Florey, Ed. (Academic, Boston, 2001), Vol. 28, pp. 1–76.
25. E. M. Ryan *et al.*, Antioxidant properties of citric acid interfere with the uricase-based measurement of circulating uric acid. *J. Pharm. Biomed. Anal.* **164**, 460–466 (2019).
26. G. Hatzivassiliou *et al.*, ATP citrate lyase inhibition can suppress tumor cell growth. *Cancer Cell* **8**, 311–321 (2005).
27. M. Robert Michaud *et al.*, Metabolomics reveals unique and shared metabolic changes in response to heat shock, freezing and desiccation in the Antarctic midge, *Belgica antarctica*. *J. Insect Physiol.* **54**, 645–655 (2008).
28. Y. N. Patil, B. Marden, M. D. Brand, S. C. Hand, Metabolic downregulation and inhibition of carbohydrate catabolism during diapause in embryos of *Artemia franciscana*. *Physiol. Biochem. Zool.* **86**, 106–118 (2013).
29. K. B. Storey, Life in the slow lane: Molecular mechanisms of estivation. *Comp. Biochem. Physiol. A Mol. Integr. Physiol.* **133**, 733–754 (2002).
30. M. P. Raveneau, A. Benamar, D. Macherel, Water content, adenylate kinase, and mitochondria drive adenylate balance in dehydrating and imbibing seeds. *J. Exp. Bot.* **68**, 3501–3512 (2017).
31. D. Garcia, R. J. Shaw, AMPK: Mechanisms of cellular energy sensing and restoration of metabolic balance. *Mol. Cell* **66**, 789–800 (2017).
32. X. Liang, L. Zhang, S. K. Natarajan, D. F. Becker, Proline mechanisms of stress survival. *Antioxid. Redox Signal.* **19**, 998–1011 (2013).
33. V. Koštál *et al.*, Physiological basis for low-temperature survival and storage of quiescent larvae of the fruit fly *Drosophila melanogaster*. *Sci. Rep.* **6**, 32346 (2016).
34. S. Calvert *et al.*, A network pharmacology approach reveals new candidate caloric restriction mimetics in *C. elegans*. *Aging Cell* **15**, 256–266 (2016).
35. M. Nourimand, C. D. Todd, Allantoin increases cadmium tolerance in Arabidopsis via activation of antioxidant mechanisms. *Plant Cell Physiol.* **57**, 2485–2496 (2016).
36. S. Jurkovič, J. Osredkar, J. Marc, Molecular impact of glutathione peroxidases in antioxidant processes. *Biochem. Med. (Zagreb)* **18**, 162–174 (2008).
37. X. Yu, Y. C. Long, Crosstalk between cystine and glutathione is critical for the regulation of amino acid signaling pathways and ferroptosis. *Sci. Rep.* **6**, 30033 (2016).
38. R. Quintana-Cabrera *et al.*, γ-Glutamylcysteine detoxifies reactive oxygen species by acting as glutathione peroxidase-1 cofactor. *Nat. Commun.* **3**, 718 (2012).
39. T. Soga *et al.*, Differential metabolomics reveals ophthalmic acid as an oxidative stress biomarker indicating hepatic glutathione consumption. *J. Biol. Chem.* **281**, 16768–16776 (2006).
40. T. Ito, M. Tokoro, R. Hori, H. Hemmi, T. Yoshimura, Production of ophthalmic acid using engineered *Escherichia coli*. *Appl. Environ. Microbiol.* **84**, e02806-17 (2018).
41. Q. Han, B. T. Beerntsen, J. Li, The tryptophan oxidation pathway in mosquitoes with emphasis on xanthurenic acid biosynthesis. *J. Insect Physiol.* **53**, 254–263 (2007).
42. D. Ramírez-Ortega *et al.*, 3-Hydroxykynurenine and 3-hydroxyanthranilic acid enhance the toxicity induced by copper in rat astrocyte culture. *Oxid. Med. Cell. Longev.* **2017**, 2371895 (2017).
43. A. Cerstiaens *et al.*, Neurotoxic and neurobehavioral effects of kynurenines in adult insects. *Biochem. Biophys. Res. Commun.* **312**, 1171–1177 (2003).
44. F. Takeuchi, R. Tsubouchi, S. Izuta, Y. Shibata, Kynurenine metabolism and xanthurenic acid formation in vitamin B6-deficient rat after tryptophan injection. *J. Nutr. Sci. Vitaminol. (Tokyo)* **35**, 111–122 (1989).
45. K. V. Sathyasaikumar *et al.*, Xanthurenic acid formation from 3-hydroxykynurenine in the mammalian brain: Neurochemical characterization and physiological effects. *Neuroscience* **367**, 85–97 (2017).
46. Q. Han, J. Fang, J. Li, 3-Hydroxykynurenine transaminase identity with alanine glyoxylate transaminase. A probable detoxification protein in *Aedes aegypti*. *J. Biol. Chem.* **277**, 15781–15787 (2002).
47. T. Soga *et al.*, Quantitative metabolome analysis using capillary electrophoresis mass spectrometry. *J. Proteome Res.* **2**, 488–494 (2003).
48. M. DuBois *et al.*, Colorimetric method for determination of sugars and related substances. *Anal. Chem.* **28**, 350–356 (1956).